


Article

Influence of the Cross-Sectional Shape of a Reinforced Bimodular Beam on the Stress-Strain State in a Transverse Impact

Alexey Beskopylny ^{1,*} , Elena Kadomtseva ², Besarion Meskhi ³, Grigory Strelnikov ² and Oleg Polushkin ⁴

¹ Department of Transport Systems, Faculty of Roads and Transport Systems, Don State Technical University, Gagarin, 1, 344000 Rostov-on-Don, Russia

² Department of the Strength of Materials, Faculty of Civil Engineering, Don State Technical University, 344000 Rostov-on-Don, Russia; elkadom@yandex.ru (E.K.); pioner0236@mail.ru (G.S.)

³ Department of Life Safety and Environmental Protection, Faculty of Life Safety and Environmental Engineering, Don State Technical University, Gagarin, 1, 344000 Rostov-on-Don, Russia; reception@donstu.ru

⁴ Department of Theoretical and Applied Mechanics, Faculty of Agribusiness, Don State Technical University, Gagarin, 1, 344000 Rostov-on-Don, Russia; o.polushkin@sci.donstu.ru

* Correspondence: besk-an@yandex.ru; Tel.: +7-863-2738454

Received: 18 October 2020; Accepted: 11 December 2020; Published: 18 December 2020



Abstract: The paper considers the stress-strain state of a reinforced concrete beam, as a bimodular material, under the action of an impact. The behavior of bimodular concretes with different moduli of elasticity in tension and compression has not been studied enough. At the same time, taking into account the bimodularity of concrete makes it possible to design a more economical structure, especially for dynamic load. In this article, the impact is considered as an absolutely plastic impact of an absolutely rigid body on an elastic system. The stress state is investigated for beams of rectangular, T-section and I-sections, and is compared with and without the bimodularity of reinforced concrete. The analysis of the dependence of the stress state on the shape, cross-sectional dimensions, and the location of reinforcing bars in the compressed and tensioned zones was carried out for lightweight concrete ($E_t < E_c$) and for heavy concrete ($E_t > E_c$) under the action of shock load with and without regard to the mass of the beam. The numerical study shows that taking into account the mass of the beam upon impact significantly decreases the magnitude of the normal stresses in both the tensioned and compressed zones. Beams of rectangular cross-section have the highest load-bearing capacity when the cross-section height is equal for both light and heavy concrete. An increase in the size of the flange of the I-beam in the stretched zone leads to a sharp decrease in normal tensile stresses and a slight increase in normal compressive stresses. The proposed engineering method makes it possible to numerically study the effect on the stress-strain state of a beam under the action of a concentrated impact of various geometric characteristics of the cross-section, bimodularity of the material, size, number and location of reinforcement.

Keywords: bimodularity; concrete; stress-strain state; reinforced beam; impact; beam shape

1. Introduction

The importance of theoretical and experimental research on the behavior of structures subjected to various types of shock impacts has attracted the attention of many scientists and practitioners to the development of methods for calculating strength and stiffness and conducting experiments to determine the degree of reliability of structures.

Dynamic effects, impacts, are the most dangerous types of loading of buildings and structures (Lyapin A. et al. [1]). However, the complexity of the calculations of structures for dynamic actions, accompanied by the solution of systems of partial differential equations, complicates the analysis of the stress-strain state (Beskopylny A. et al. [2], He X-T. et al. [3]). For heterogeneous materials, the problems are considered mainly numerically (Cai K. et al. [4]).

Goldsmith W. in his book “Impact. The theory and physical properties of colliding bodies” [5] gives the study of impact in its classical formulation. The fundamental foundations of wave processes during impact and methods for solving partial differential equations describing processes during impact are considered. An important part of the book is devoted to the description of the technique of the experimental study of shock and wave processes.

A special type of impact on elements of reinforced concrete structures is the so-called emergency shock load, for example, Borys S. et al. [6], Krašna S. et al. [7], Furtado A. et al. [8], Safi W.A. et al. [9] and others, since they are characterized by high intensity and rare repeatability. An accidental impact can occur, for example, when erecting a multistory building or a multitiered or high structure in the event of an emergency break of a sling, careless securing of a load, the careless turning of the crane boom, etc. The numerical modelling of the impact penetration of a steel cylindrical object into a concrete structure is considered in the work of Belov N. et al. [10]. The impact of a steel body on a concrete column was simulated with an initial velocity of 1 km/s in the longitudinal and transverse directions.

According to various estimates (Wu X. et al. [11]), losses from accidental strikes range from tens to hundreds of millions of dollars a year. They are also often accompanied by the death of people. Most emergency strikes are delivered by bodies (strikers) of significant mass (up to several tons) at relatively low speeds (1–20 m/s). From the standpoint of the reaction of the structure, this distinguishes emergency strikes from the high-speed strikes of bombs and projectiles on protective structures, well-studied by military engineers, since it allows the use of methods based on the concepts of classical dynamics for calculations (Buzyurkin A. et al. [12]).

When analyzing the deformation of individual reinforced concrete elements subjected to an emergency impact, it is necessary to consider the local and general effect of the impact. Local action is understood as the primary impact effect that causes local damage and destruction in the structure (penetration of the striker into the structure, as well as spalling and punching), usually before significant general deformations appear. The general impact of an impact means its secondary effect, which causes general deformations of the structure (bending, etc.).

The analysis of the general deformation of reinforced concrete beams under shock loading showed that, as in the case of static and impulsive actions, the sections of elements during loading go through three stages: before cracking in the tension zone; after cracking until reaching the yield point in tension reinforcement; after reaching the yield point to failure. Accordingly, three stages of beam operation can be considered: no cracks; conditionally elastic with cracks in the stretched zone of sections (until yield in tensioned reinforcement is achieved; plastic (or elastic-plastic) after reaching yield in reinforcement. Pan K. et al. [13] measured crack propagation rates in three types of self-compacting steel fiber-reinforced concrete. Different loading rates were simulated experimentally for three-point bending. An increase in the ability to absorb energy is noted with increasing fiber content.

Li Y. et al. [14], concrete specimens were tested for shock compression under various thermal effects of the freeze-thaw cycle using the Hopkinson installation. Then the dynamic crack morphology, crack block distribution, stress-strain curve, maximum stress and other dynamic mechanical properties of concrete were studied. The process of damage development and the mechanism of freezing thawed concrete materials were investigated.

High strain rates can significantly change the mechanical properties of concrete. Yu X. et al. [15] proposed a method for assessing the basic properties of conventional concrete at high strain rates. The proposed method combined the inverse Lagrangian analysis method with optical methods using an ultra-high speed camera and digital image correlation methods. Dynamic tests showed the nonlinear

behavior of stress-strain curves. In our opinion, this could be explained both by the local heterogeneity of concrete and by inertial forces upon impact.

Zhai Y. et al. [16] experimentally investigated the mechanical characteristics in compression of various heat-treated (400–800 °C) concrete specimens at the Hopkinson installation. It was shown that in uniaxial testing, with an increase in the impact velocity, the crack initiation time increased, and the degree of fracture increased at the same rate as the loading time.

Experimental research (Radchenko A. et al. [17]) for the action of a dynamic load have shown that the actual design diagram of the deformation of a reinforced concrete structure depended not only on the intensity of the dynamic load, as discussed in previous paragraphs. The influence of the cross-sectional shape of the element, the classes of concrete and reinforcement, the percentage of beam reinforcement were also significant. In Beskopylny A. et al. [18], the influence of different moduli of elasticity of the material on the stress state of the column in the compressed and stretched parts was investigated. It was shown that in some cases normal tensile stresses without bimodularity were 46% less than with bimodularity, and normal compressive stresses were 29% higher than those with bimodularity. In article [19] Beskopylny A. et al. considered a reinforced concrete beam made of bimodular material on an elastic Winkler foundation. The influence of the number of reinforcing bars located in the tensile zone on the maximum normal stress and maximum deflection was studied numerically.

The widespread use of reinforced concrete elements in various building structures subjected to static and dynamic loads makes it necessary to develop theoretical methods for calculating strength and stiffness, taking into account the mechanical characteristics of various types of concrete. An important property of concrete is bimodularity, that is, the difference in elastic moduli and Poisson's ratios in tension and compression. For some types of fine-grained concrete, the modulus of elasticity in tension is two to three times less than in compression, for example, concrete AFB-1 (reinforced fiber concrete #1): $E_c = 1.75 \cdot 10^4$ MPa, $E_t = 0.75 \cdot 10^4$ MPa [20], fiber-reinforced concrete: $E_c = 2.25 \cdot 10^3$ MPa; $E_t = 5 \cdot 10^3$ MPa [20].

Starting with the fundamental works of Ambartsumyan S. [20–22], Jones R. [23], Bert C. [24], the theory of bimodular materials began to develop actively. Zolochovsky A. et al. [25–27] developed a theory of creep for materials with different moduli under tension and compression. A constitutive creep strain model that described the load-history-dependent behavior of initially isotropic materials with different tensile and compressive properties was presented. The model was based on kinematic hardening and introduced effective equivalent stress into the creep potential, which was based on the first and second invariants of the effective stress tensor. Practical calculations were carried out numerically.

Analytical solutions for functionally variable curved beams with different properties in tension and compression, in which the moduli of elasticity in tension and compression were taken as two different exponential functions were obtained by He X. et al. [28–31]. The authors identified an unknown neutral layer and created a simplified mechanical model related to the tension and compression subzone. Combining the boundary conditions with the conditions of continuity of the neutral layer, the authors applied the power series method to solve the stress components in pure bending. Variations of radial and circumferential stresses in various cases of bimodular functional-gradient parameters were analyzed using numerical examples.

Li X. in [32] considered a beam made of functionally variable material with characteristics having different moduli of elasticity in tension and compression. One-dimensional and two-dimensional mechanical models for a functionally gradient beam with a bimodular effect were obtained. It was shown that, due to the introduction of the bimodular functional-gradient effect of materials, the maximum tensile and compressive bending stresses might not occur in the lower and upper parts of the beam but were determined using an extreme condition for an analytical solution.

The above review shows that the development of models for structures made of bimodular materials is an important scientific problem. The behavior of structural elements made of bimodular materials can significantly change the stress-strain state in comparison with materials with bimodularity.

The stress-strain state of structures made of bimodular materials is practically not observed under shock loading. Thus, the main goal of the article is to develop a mathematical model for a reinforced concrete beam, taking into account bimodularity, and to assess the influence of the cross-sectional shape during transverse impact.

2. Materials and Methods

The paper considers a simply supported reinforced beam made of bimodular material. A load falls onto the beam from a height h in the middle of the span. The impact is considered as an absolutely plastic impact of an absolutely rigid body against an elastic system, taking into account the hypothesis about the proportionality of the dynamic and static characteristics of the stress-strain state of the body. The general impact of the impact is considered, i.e., is determined by the stress-strain state of a reinforced concrete beam before cracks appear in concrete and the development of plastic deformations in reinforcement.

The design scheme of the beam is shown in Figure 1. The problem is solved in a general way. Section dimensions are taken as an example based on typical designs.

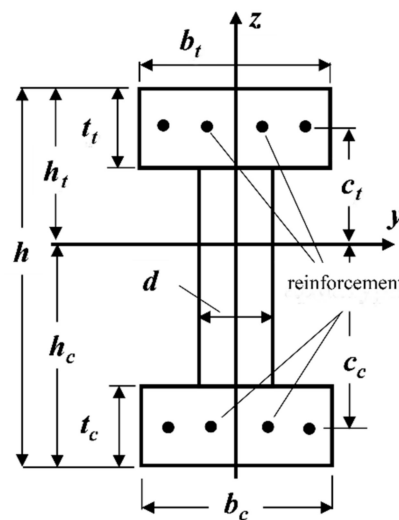


Figure 1. Calculation scheme: (b_t) beam width in tension zone; (b_c) beam width in the compressed zone; (h) , (h_t) , (h_c) beam height, beam height in tension and compressed zones; (t_t) , (t_c) the dimensions of the flanges in the stretched and compressed zones; (d) web width.

Cross-sectional dimensions (Figure 1)

(a) I-beam

$$h = 0.9 \text{ m}, b_t = 0.3 \text{ m}, t_t = 0.15 \text{ m}, d = 0.10 \text{ m}, b_c = 0.3 \text{ m}, t_c = 0.08 \text{ m};$$

(b) Rectangle

$$h = 0.9 \text{ m}, b = 0.3 \text{ m};$$

(c) T-beam

$$h = 0.9 \text{ m}, b_t = 0.1 \text{ m}, t_t = 0.15 \text{ m}, d = 0.10 \text{ m}, b_c = 0.3 \text{ m}, t_c = 0.08 \text{ m};$$

$$E_a = 2.06 \cdot 10^6 \text{ MPa}, d_t = 12 \text{ mm}, d_c = 8 \text{ mm}$$

d_t —the diameter of the reinforcement in the tension zone; c_t —the distance from the reinforcement in the tension zone to the neutral axis; n_t —the number of rods in the tension zone; d_c —the diameter of the reinforcement in the compression zone; c_c —distance (coordinate) from the reinforcement in the compression zone to the neutral axis; n_c —number of rods in the compression zone.

In this paper, we consider beams made of fiber-reinforced concrete (lightweight concrete), $L = 4 \text{ m}$, density $\rho = 700 \text{ kg/cm}^3$, and AFB-1 (heavy concrete), density $\rho = 2000 \text{ kg/cm}^3$, with cross-sections in the form of a rectangle, T-beam and I-beam. The corresponding reduced masses of beams M_B are equal for beams made of fiber-reinforced concrete of rectangular cross-section $M_{B1} = 367.2 \text{ kg}$,

T-section $M_{B2} = 163.2$ kg and I-beam cross-section $M_{B3} = 184.96$ kg, from AFB-1 $M_{B4} = 1049$ kg, $M_{B5} = 466.3$ kg and $M_{B6} = 528.5$ kg.

The values of the load and the mass of the beams were chosen in such a way that the dynamic coefficient was not equal to 2. With the value of the falling weight equal to 100 kg for beams made of fiber-reinforced concrete for a rectangular cross-section $m_B L/M_A = 7.71$, a T-cross section $m_B L/M_A = 3.423$, an I-cross section $m_B L/M_A = 3.9$. For fiber-reinforced concrete beams of rectangular cross-section $m_B L/M_A = 22$, T-section $m_B L/M_A = 9.77$ and I-section cross-section $m_B L/M_A = 11.1$.

The dynamic coefficient is determined by the formulas [33]:

- (a) without considering the mass of the beam, Equation (1):

$$k_d = 1 + \sqrt{1 + \frac{2h}{f_s}} \quad (1)$$

- (b) considering the mass of the beam, Equation (2):

$$k_d = 1 + \sqrt{1 + \frac{2h}{f_s} \left(1 + \frac{M_B}{M_A}\right)^{-3}} \quad (2)$$

where h is the height of the fall of the load; f_s is the static deflection of the beam under load without taking into account the mass of the beam; M_A is the mass of the falling weight, M_B is the reduced mass of the beam according to Cox H. [33]. For a simply supported beam, loaded in the middle of the span, $M_B = \frac{17}{35} m_B L$ where m_B is the distributed mass of the beam, L is the beam length.

The change in the coefficient k_d (Equations (1) and (2)) depending on whether the mass of the beam is taken into account is shown in Figure 2.

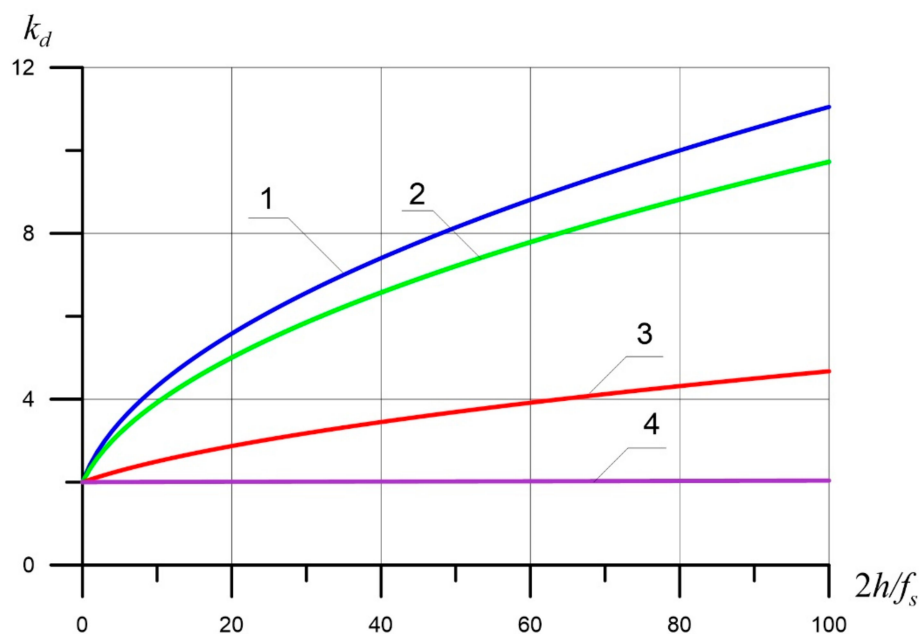


Figure 2. Dependence of the dynamic coefficient k_d on the relative height of the beam section $2h/f_s$ at various ratios of the beam mass to the mass of the falling load M_B/M_A : (1) $M_B/M_A = 0$; (2) $M_B/M_A = 0.1$; (3) $M_B/M_A = 1.0$; (4) $M_B/M_A = 100.0$.

Figure 2 shows the dependence of the dynamic coefficient k_d on the relative height of the beam section $2h/f_s$ at various ratios M_B/M_A . Curve 1 corresponds to $M_B/M_A = 0$, curve 2 corresponds to

$M_B/M_A = 0.1$, curve 3 corresponds to $M_B/M_A = 1$, curve 4 corresponds to $M_B/M_A = 100$. The static deflection f_s was determined without considering the bimodularity of the beam material. As can be seen from Figure 2, the dynamic coefficient k_d reaches its highest value at $M_B/M_A = 0$ (Curve 1), which corresponds to the case if the beam mass is not taken into account in the calculations.

If the mass of the beam is significantly greater than the mass of the falling load ($M_B \gg M_B$, curve 4), then the dynamic coefficient is the constant $k_d = 2$.

The Formula (2) determines normal dynamic stresses arising in the cross-section of the beam: $\sigma_{dt} = k_d \cdot \sigma_t$, $\sigma_{dc} = k_d \cdot \sigma_c$, $\sigma_{da} = k_d \cdot \sigma_a$, where σ_{dt} , σ_{dc} , σ_{da} , respectively, dynamic normal stresses arising in the tensile, compressed zone of the material beams and reinforcement; σ_t , σ_c , σ_a , respectively, static normal stresses arising in the tensioned, compressed zone of the material of the beam and the reinforcement.

Static stresses and deflection are determined from the action of a statically applied force in the middle of the span, taking into account the bimodularity of the material of the reinforced beam.

A model of a reinforced beam made of a bimodular material was considered as a beam consisting of rigidly connected layers with different mechanical characteristics, in particular, different moduli of elasticity for tension and compression of the material of the beam and reinforcement bars. In this case, the beam became statically indeterminate concerning internal bending moments that arise in the tensioned, compressed zones of the beam material and the reinforcement bars [34–37].

Under these assumptions, the bending moment appearing in the cross-section of the beam has the form

- (a) equilibrium equation for a heterogeneous beam, Equation (3):

$$M_y = M_{yt} + M_{yc} + M_{ya} \quad (3)$$

- (b) deformation compatibility condition of a heterogeneous beam, Equation (4):

$$\frac{1}{\rho} = \frac{1}{\rho_t} = \frac{1}{\rho_c} = \frac{1}{\rho_a} \quad (4)$$

where $M_y, \frac{1}{\rho}$ is the bending moment and beam curvature; $M_{yt}, \frac{1}{\rho_t}$ is the bending moment and curvature of the tensile zone beam; $M_{yc}, \frac{1}{\rho_c}$ is bending moment and curvature of the compressed zone beam; $M_{ya}, \frac{1}{\rho_a}$ is bending moment and curvature of rebars.

The equilibrium condition $\sum M_y = 0$, expressed in terms of normal stresses, has the form, Equation (5):

$$M_y = \int_A \sigma z dA = \int_A \sigma_t z dA + \int_A \sigma_c z dA + \int_A \sigma_a z dA = M_{yt} + M_{yc} + M_{ya} \quad (5)$$

where σ_t, A_t are the normal stress and the cross-sectional area of the beam in the tensile zone, σ_c, A_c are the normal stress and the cross-sectional area of the beam in the compression, compression zone, σ_a, A_a are the normal stress and the cross-sectional area of the reinforcement.

The formulas for normal stresses arising in the cross-section of a beam are, Equation (6):

$$\sigma_t = \frac{E_t z}{\rho}, \sigma_c = \frac{E_c z}{\rho}, \sigma_a = \frac{E_a z}{\rho} \quad (6)$$

Substituting the normal stress Formula (6) in (5), we obtain the formula for determining the curvature of the neutral line for a reinforced beam made of bimodular material, Equation (7):

$$M_y = \frac{1}{\rho} [E_t J_y^t + E_c J_y^c + E_a (n_t (J_{y1}^t + A_a^t c_t^2) + n_c (J_{y1}^c + A_a^c c_c^2))] \quad (7)$$

For the beam, we have the general curvature formula, Equation (8):

$$\frac{1}{\rho} = \frac{M_y}{D} = \frac{M_{yt} + M_{yc} + M_{ya}}{D} \quad (8)$$

where D is the reduced stiffness of a reinforced beam made of bimodular material; E_t is the tensile modulus of the material; E_c is the elastic modulus of the material under compression; E_a is the tensile modulus of reinforcement; J_y^t is the moment of inertia about the neutral axis of the part of the cross-section that lies in the tension zone; J_y^c is the moment of inertia about the neutral axis of the part of the cross-section that lies in the compression zone; J_{y1}^t is the moment of inertia of the cross-section of the reinforcement, which lies in the tension zone, relative to its own central axis; J_{y1}^c is the moment of inertia of the cross-section of the reinforcement, which lies in the compression zone, relative to its own central axis; n_t is the number of reinforcement bars in the tension zone; n_c is the number of reinforcement bars in the compression zone; A_a^t is the cross-sectional area of the reinforcement in the tension zone; A_a^c cross-sectional area of reinforcement in the compression zone; c_t distance from the reinforcement in the tension zone to the neutral axis; c_c is the distance from the reinforcement in the compression zone to the neutral axis.

Comparing Formulas (7) and (8), we obtain the expression for the reduced stiffness D for reinforced beams made of bimodal material, Equation (9):

$$D = E_t J_y^t + E_c J_y^c + E_a [n_t (J_{y1}^t + A_a^t c_t^2) + n_c (J_{y1}^c + A_a^c c_c^2)] \quad (9)$$

To determine the position of the neutral line (to determine the height of the stretching and compressed zones), consider the equilibrium equations, Equations (10) and (11):

$$\sum X = 0, \sum M_z = 0 \int_{A_t} \sigma_t dA + \int_{A_c} \sigma_c dA + \int_{A_a} \sigma_a dA = 0 \quad (10)$$

$$\int_{A_t} \sigma_t y dA + \int_{A_c} \sigma_c y dA + \int_{A_a} \sigma_a y dA = 0 \quad (11)$$

After substituting (6) into (10), (11), we obtain, Equations (12) and (13):

$$E_t S_{yt} + E_c S_{yc} + E_a S_{ya} = 0 \quad (12)$$

$$E_t I_{yzt} + E_c I_{yzc} + E_a I_{yza} = 0 \quad (13)$$

where S_{yt} is the static moment of the cross-sectional area of the expanding zone relative to the neutral line, S_{yc} is the static moment of the cross-sectional area of the contracting zone relative to the neutral line, S_{ya} is the static moment of the area of reinforcement bars relative to the neutral line

Equations (12) and (13) are used to determine the neutral line of the cross-section of beams with an arbitrary cross-section.

Centrifugal moments of inertia $I_{yzt}(x) = 0$, $I_{yzc}(x) = 0$ since the cross-section is considered symmetric about the y-axis. Then Equation (13) is satisfied identically, and the position of the neutral line is determined from Equation (12).

For a rectangular beam (12) is written in the following form, Equation (14):

$$(h_t)^2 + 2 \frac{k}{1-k} h h_t - \frac{k}{1-k} (h)^2 + \frac{2E_a}{b(1-k)E_t} S_{ya} = 0 \quad (14)$$

The positive root of which has the form ($k \neq 1$), Equation (15):

$$h_t = -\frac{k}{1-k}h + \sqrt{\frac{k}{(1-k)^2}(h)^2 - \frac{2E_a}{b(1-k)E_t}S_{ya}} \quad (15)$$

The height of the compressed zone h_c is found from the condition $h = h_c + h_t$, Equation (16):

$$h_c = -\frac{k}{1-k}h - \sqrt{\frac{k}{(1-k)^2}(h)^2 - \frac{2E_a}{b(1-k)E_t}S_{ya}} \quad (16)$$

where h_c is the height of the compressed area; h_t is the height of the stretched area, h is the height of the cross-section, b is the width of the cross-section $\frac{E_c}{E_t} = k$.

For I-beams and T-beams, expression (12) has the form, Equation (17):

$$a h_c^2 + b_1 h_c + c = 0 \quad (17)$$

where $a = \frac{d}{2}(1-k)$; $b_1 = [k d t_c - d(h - t_t) - b_t t_t - k b_c t_c]$

$$c = \frac{d}{2}(h - t_t)^2 - k \frac{d}{2} t_c^2 + b_t t_t \left(h - \frac{t_t}{2} \right) + k b_c \frac{t_c^2}{2} + (n_c c_c A_c + n_t c_t A_t) \frac{E_a}{E_t}$$

where d is the wall thickness of the cross-section, b_t , t_t are the width and thickness of the cross-section flange in the tension zone, b_c , t_c are the width and thickness of the cross-section flange in the compression zone, n_c , c_c are the number and distance to the neutral line of reinforcing bars in the compressed zone, n_t , c_t are the the number and distance to the neutral line of reinforcing bars in the tensioned zone, A_c , A_t are the cross-sectional areas of the reinforcing bars in the compressed and tensile zones, respectively.

The formulas for normal stresses arising in the cross-sections of a beam under the action of static loads, taking into account (6), (8), have the form, Equation (18):

$$\sigma_t = \frac{E_t M_y}{D} z, \quad \sigma_c = \frac{E_c M_y}{D} z, \quad \sigma_a = \frac{E_a M_y}{D} z \quad (18)$$

where z is the distance from the neutral line to the point at which the normal voltage is determined.

3. Results

In the example of a simply supported beam with various cross-sectional shapes, rectangle, I-beam and T-beam, the values of the maximum compressive and tensile dynamic normal stresses arising from the action of a falling load with a mass of $M_A = 100$ kg from a height $h = 4.00$ cm to the middle of a reinforced beam made of a bimodular material were calculated.

Various options for the most optimal technological necessity of using reinforced concrete beams of different cross-sectional shapes with equal height and width of the shelves were considered (Figure 3).



Figure 3. Examples of simply supported reinforced concrete beams of T, I, and rectangular cross-sections used in building structures.

3.1. A Fiber-Reinforced Concrete Beam

Elastic moduli $E_c = 2.25 \cdot 10^3$ MPa; $E_t = 5.0 \cdot 10^3$ MPa. Drop weight $M_A = 100$ kg; drop height: $h = 4$ cm, the number of reinforcement bars $n_t = 2$, $n_c = 2$. Maximum dynamic stresses arising in beams of rectangular, T- and I-shape, considering bimodularity are presented in Table 1.

Table 1. Maximum dynamic stresses in beams of rectangular, T- and I-shape, considering bimodularity. $n_t = 2$, $n_c = 2$, $E_t = 5000$ MPa; $E_c = 2250$ MPa.

Beam Material	Sectional Shape					
	Rectangular		T-Beam		I-Beam	
Fiber-foam concrete material	σ_{dt} , MPa	σ_{dc} , MPa	σ_{dt} , MPa	σ_{dc} , MPa	σ_{dt} , MPa	σ_{dc} , MPa
Without considering the mass of the beam	1.685	1.157	1.708	1.824	1.711	1.489
Considering the mass of the beam	0.192	0.132	0.428	0.457	0.381	0.332

With the same height of the rectangular, I-beam, and T-cross-sections, the largest maximum tensile stress occurred in the I-beam, without taking into account the mass, although it differed from the maximum normal tensile stresses that arose in the rectangle and T-bar within 1.55%. The maximum compressive stress under the same conditions occurred in the T-bar and differed from the same stresses in the I-beam and rectangle within 58%.

Considering the mass of the beams, the values of the maximum normal stresses were reduced for a rectangle by 778%, for a T-beam by 299%, for an I-beam by 349%. The highest normal tensile stress in a tee was two times greater than in a rectangular cross-section and 1.2 times more than in an I-beam.

The smallest maximum stresses arose in a rectangular cross-section with and without regard to the mass of the beam and taking into account the mass of the beam, the largest nominal stresses in absolute magnitude arose in the T-bar. Maximum dynamic stresses arising in a beam of rectangular, T-shaped and I-beams, without bimodularity are presented in Table 2.

Table 2. Maximum dynamic stresses arising in beams of rectangular, T- and I-shape, without bimodularity. $E_t = 5000$ MPa; $E_c = 5000$ MPa.

Beam Material	Sectional Shape					
	Rectangular		T-Beam		I-Beam	
Fiber-foam concrete material	σ_{dt} , MPa	σ_{dc} , MPa	σ_{dt} , MPa	σ_{dc} , MPa	σ_{dt} , MPa	σ_{dc} , MPa
Without considering the mass of the beam	1.710	1.770	1.825	2.876	1.828	2.243
Considering the mass of the beam	0.190	0.197	0.452	0.712	0.402	0.493

The qualitative picture of the ratios of the maximum normal stress stresses with and without bimodularity did not change, but the absolute value of the maximum normal stresses was higher when

bimodularity was taken into account: for a rectangle, σ_{dt} increased by 1.5%, σ_{dc} increased by 53%; for a T-beam σ_{dt} increased by 8%, σ_{dc} increased by 58%; for an I-beam, σ_{dt} increased by 7%, σ_{dc} increased by 51%.

3.2. AFB-1 Concrete Beam

Elastic moduli $E_c = 2.25 \cdot 10^3$ MPa; $E_t = 1.75 \cdot 10^4$ MPa. Drop weight $M_A = 100$ kg; drop height: $h = 4$ cm, the number of reinforcement bars $n_t = 2$, $n_c = 2$. Maximum dynamic stresses arising in beams of rectangular, T- and I-shape, with bimodularity are presented in Table 3.

Table 3. Maximum dynamic stresses in beams of rectangular, T- and I-shape, considering bimodularity $n_t = 2$, $n_c = 2$, $E_t = 17500$ MPa; $E_c = 7500$ MPa.

Beam Material	Sectional Shape					
	Rectangular		T-Beam		I-Beam	
Fiber-foam concrete material	σ_{dt} , MPa	σ_{dc} , MPa	σ_{dt} , MPa	σ_{dc} , MPa	σ_{dt} , MPa	σ_{dc} , MPa
Without considering the mass of the beam	2.157	3.379	2.439	5.585	2.438	4.106
Considering the mass of the beam	0.077	0.120	0.210	0.480	0.180	0.303

An increase in the value of the elastic moduli led to an increase in the value of the maximum normal stresses (Table 2), and σ_{dc} was greater than σ_{dt} , in contrast to beams made of fiber-reinforced concrete (Table 1). In concrete beams AFB-1, the largest maximum normal stresses occurred in the T-bar, the smallest in the rectangular cross-section. For fiber-reinforced concrete beams, σ_{dt} was greater than σ_{dc} , while for a lightweight concrete beam, σ_{dt} was less than σ_{dc} . Maximum dynamic stresses arising in beams of rectangular, T- and I-shape, without bimodularity are presented in Table 4.

Table 4. Maximum dynamic stresses arising in beams of rectangular, T- and I-shape, without bimodularity. $E_t = 7500$ MPa; $E_c = 7500$ MPa.

Beam Material	Sectional Shape					
	Rectangular		T-Beam		I-Beam	
Fiber-foam concrete material	σ_{dt} , MPa	σ_{dc} , MPa	σ_{dt} , MPa	σ_{dc} , MPa	σ_{dt} , MPa	σ_{dc} , MPa
Without considering the mass of the beam	2.143	2.193	2.315	3.611	2.310	2.790
Considering the mass of the beam	0.081	0.083	0.205	0.320	0.176	0.212

Taking into account the bimodularity for beams made of heavy concrete reduces the values of maximum normal stresses (Tables 3 and 4), in contrast to beams made of fiber-reinforced concrete (Tables 1 and 2) σ_{dt} decreases within 5%, σ_{dc} decreases within 55%, both with regard to the mass of the beam and without taking into account the mass of the beam.

3.3. A Fiber Concrete Beam Reinforced in the Tensile Zone

Elastic moduli $E_c = 2.25 \cdot 10^3$ MPa; $E_t = 5.0 \cdot 10^3$ MPa. Drop weight $M_A = 100$ kg; drop height: $h = 4$ cm, the number of reinforcement bars $n_t = 2$, $n_c = 0$. Consider the influence of the location of the reinforcement on the value of the maximum dynamic normal stresses. Maximum dynamic stresses arising in a beam of rectangular, T-shaped and I-beams, considering bimodularity are presented in Table 5.

Table 5. Maximum dynamic stresses arising in beams of rectangular, T- and I-shape, considering bimodularity. $n_t = 2, n_c = 0, E_t = 5000 \text{ MPa}; E_c = 2250 \text{ MPa}$.

Beam Material	Sectional Shape					
	Rectangular		T-Beam		I-Beam	
Fiber-foam concrete material	$\sigma_{dt},$ MPa	$\sigma_{dc},$ MPa	$\sigma_{dt},$ MPa	$\sigma_{dc},$ MPa	$\sigma_{dt},$ MPa	$\sigma_{dc},$ MPa
Without considering the mass of the beam	1.834	1.168	1.942	1.826	1.934	1.485
Considering the mass of the beam	0.210	0.134	0.488	0.459	0.432	0.332

The arrangement of reinforcing bars only in the tensioned zone (Table 5) practically did not change the magnitude of the maximum compressive stresses compared to the arrangement of reinforcing bars in both the tensioned and compressed zones (Table 1). The magnitude of the maximum tensile stresses increased within 14%, both taking into account, and without taking into account the mass of the beam.

3.4. Influence of the Width b_t and the Thickness of the Flange t_t of the I-Beam on the Values of the Maximum Normal Stresses

Consider a fiber-reinforced concrete beam with elastic moduli $E_c = 2.25 \cdot 10^3 \text{ MPa}; E_t = 5.0 \cdot 10^3 \text{ MPa}$. Drop weight $M_A = 100 \text{ kg}$, drop height: $h = 4 \text{ cm}$, the number of reinforcement bars $n_t = 2, n_c = 2$. Section dimensions: $h = 90 \text{ cm}, b_t = 30 \text{ cm}, b_c = 30 \text{ cm}, t_t = 8 \text{ cm}, t_c = 8 \text{ cm}, d_c = 10 \text{ cm}$. Dependences of dynamic stresses on the width of the I-beam flange b_t are shown in Figure 4.

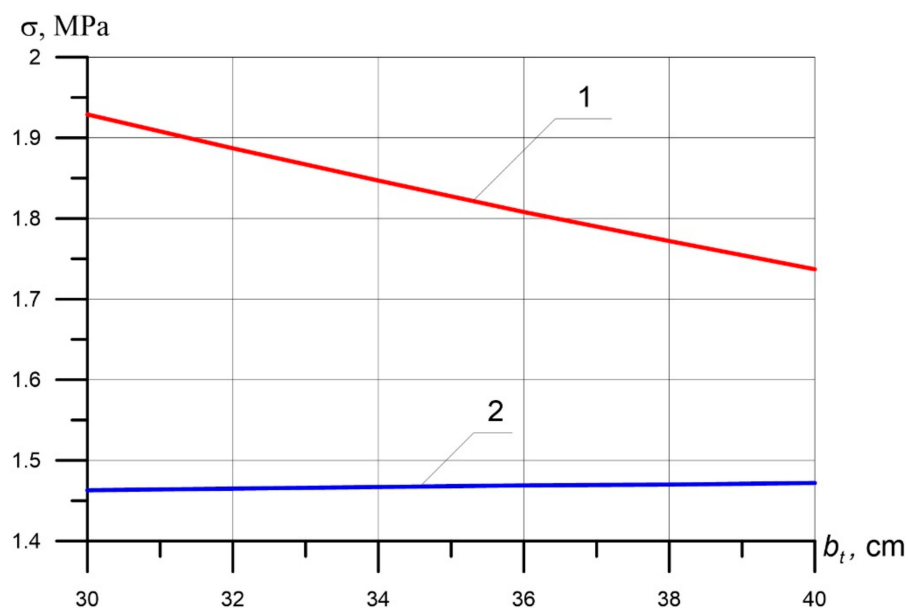


Figure 4. Dependences of dynamic stresses on the width of the I-beam flange b_t in the tension zone without taking into account the mass of the fiber-reinforced concrete beam: (1) dynamic tensile stress; (2) dynamic compressive stress.

As can be seen from the graph shown in Figure 4, an increase in the flange length b_t practically did not affect the maximum compressive stress. The maximum tensile stress decreased in direct proportion to the increase in the flange length of the stretched zone.

Dependences of dynamic stresses on the thickness of the I-beam flange t_t are shown in Figure 5.

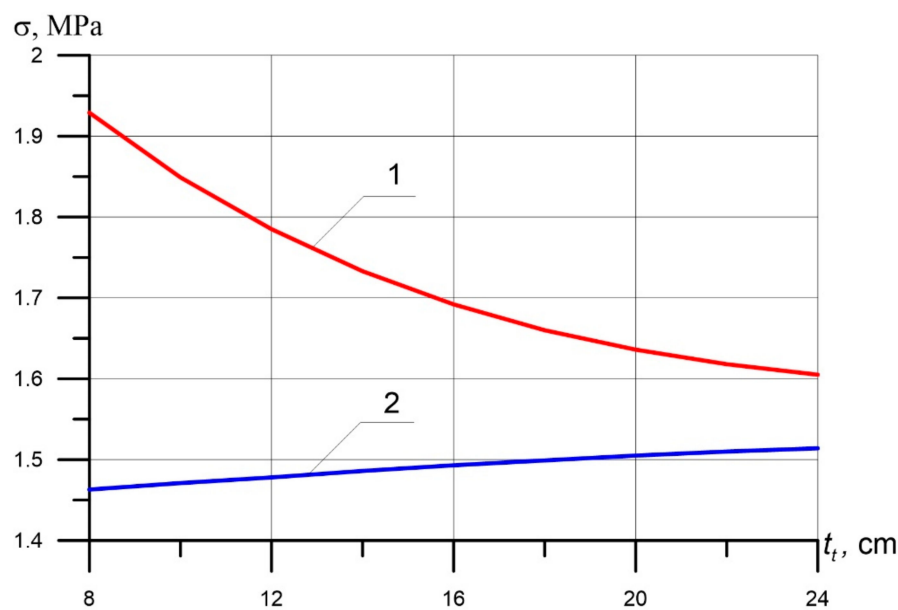


Figure 5. Dependences of dynamic stresses on the thickness of the I-beam flange t_t in the tension zone without taking into account the mass of the fiber-reinforced concrete beam, (1) dynamic tensile stress; (2) dynamic compressive stress.

From the graph shown in Figure 5 it can be seen that with an increase in the thickness of the flange of the I-beam by three times, the maximum compressive stress increased by 4%, while the maximum tensile stress decreased by 21%.

3.5. Influence of the Dimensions of the Bottom Flange, the Number of Reinforcing Bars in the Tensioned Zone and the Elastic Moduli on the Value of the Maximum Tensile and Compressive Normal Stresses Upon Impact in the Example of an I-Beam

The failure of concrete in reinforced beams begins at the points of the cross-section at which the maximum principal stress occurs, equal to the maximum tensile normal stress σ_{dt} (Figure 6). Therefore, it is important to know how the cumulative consideration of various geometrical and mechanical factors influences the values of the maximum tensile and compressive normal stresses upon impact arising in the cross-sections of the beam.



Figure 6. Destruction of a simply supported reinforced concrete beam under the action of concentrated forces.

The dependences of the dynamic normal stresses on the width of the I-beam flange b_t and the number of reinforcement bars in the tension zone of a fiber-reinforced concrete beam, taking into account the beam mass and bimodularity, are shown in Figure 7 and Table 6.

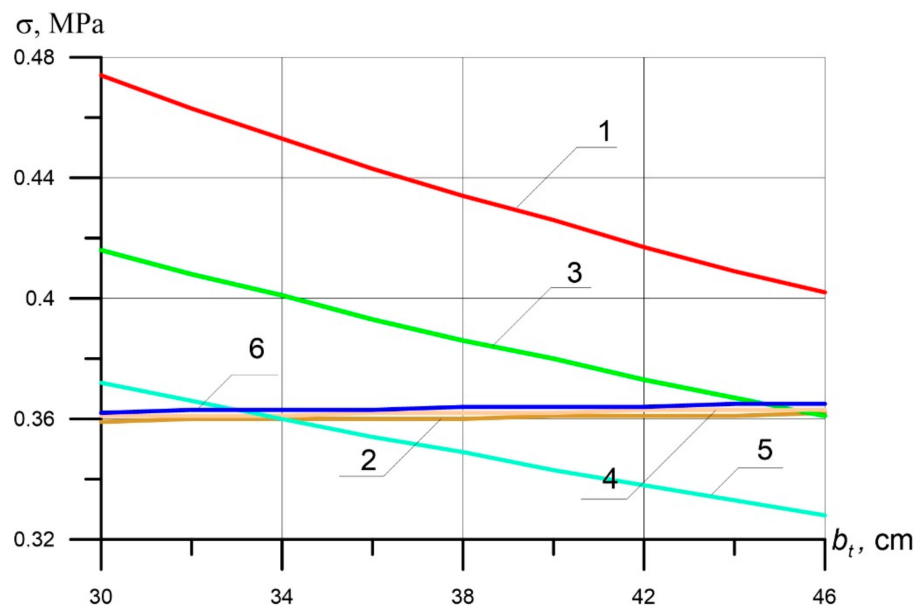


Figure 7. Dependences of dynamic normal stresses on the width of the I-beam flange b_t and the number of reinforcement rods in the tension zone of a fiber-reinforced concrete beam taking into account the beam mass and bimodularity at $n_c = 2$, $E_c = 2250$ MPa, $E_t = 5000$ MPa: (1) dynamic tensile stresses at $n_t = 2$; (2) dynamic compressive stress at $n_t = 2$; (3) dynamic tensile stresses at $n_t = 4$; (4) dynamic compressive stress at $n_t = 4$; (5) dynamic tensile stresses at $n_t = 6$; (6) dynamic compressive stresses at $n_t = 6$.

Table 6. Dependences of dynamic normal stresses on the width of the I-beam flange b_t and the number of reinforcement bars in the tension zone of a fiber-reinforced concrete beam, taking into account the beam mass and bimodularity at $n_c = 2$.

Flange Width		$n_t=2$		$n_t=4$		$n_t=6$	
b_t , cm		σ_{dt} , MPa	σ_{dc} , MPa	σ_{dt} , MPa	σ_{dc} , MPa	σ_{dt} , MPa	σ_{dc} , MPa
30		0.474	0.359	0.416	0.361	0.372	0.362
32		0.463	0.36	0.408	0.361	0.366	0.363
34		0.453	0.36	0.401	0.361	0.36	0.363
36		0.443	0.36	0.393	0.362	0.354	0.363
38		0.434	0.36	0.386	0.362	0.349	0.364
40		0.426	0.361	0.38	0.362	0.343	0.364
42		0.417	0.361	0.373	0.363	0.338	0.364
44		0.409	0.361	0.367	0.363	0.333	0.365
46		0.402	0.362	0.361	0.363	0.328	0.365

Increasing the size of the flange of the I-beam and the number of reinforcing bars located in the tensile zone reduced the dynamic normal tensile stresses and practically did not affect the value of the dynamic normal compressive stresses (Figure 6, Table 6). Increasing b_t by 53% reduced σ_{dt} by 18% with a constant number of reinforced bars. An increase in the number of reinforced bars by a factor of 3 reduced σ_{dt} by 27% at a constant flange size. A simultaneous increase in the size of the shelf by 1.8 times and an increase in the number of reinforced flanges by 3 times reduced σ_{dt} by 45%, while σ_{dc} increased by only 1.6% (Figure 6, Table 6).

Dependences of dynamic normal stresses on the width of the I-beam flange b_t and the number of reinforcement bars in the tension zone of a fiber-reinforced concrete beam, taking into account the mass of the beam and excluding bimodularity, are shown in Figure 8 and Table 7.

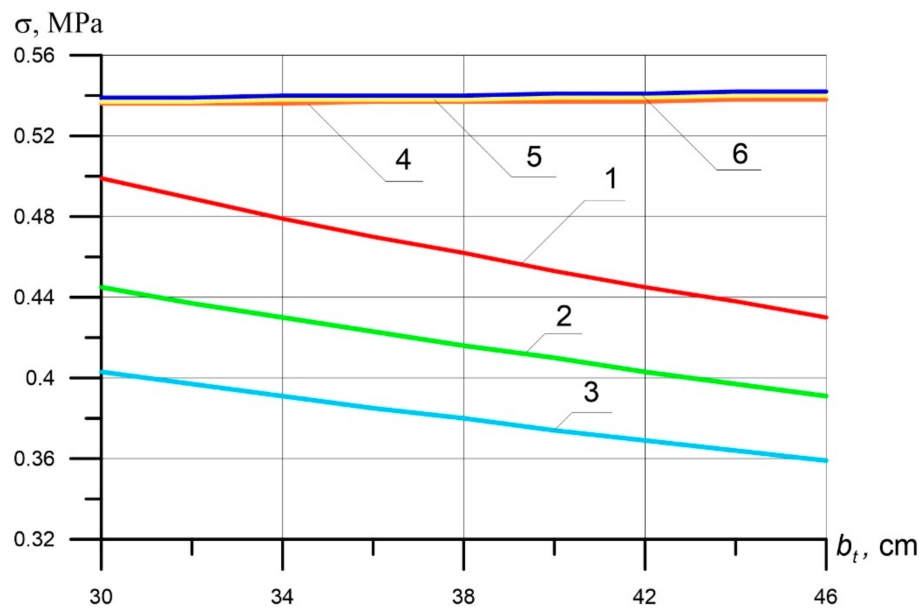


Figure 8. Dependence of dynamic normal stresses on the width of the I-beam flange b_t and the number of reinforcement rods in the tension zone of a fiber-reinforced concrete beam, taking into account the mass of the beam and without taking into account the bimodularity at $n_c = 2$, $E_c = 5000$ MPa, $E_t = 5000$ MPa: (1) dynamic tensile stresses at $n_t = 2$; (2) dynamic compressive stress at $n_t = 2$; (3) dynamic tensile stresses at $n_t = 4$; (4) dynamic compressive stress at $n_t = 4$; (5) dynamic tensile stresses at $n_t = 6$; (6) dynamic compressive stresses at $n_t = 6$.

Table 7. Dependences of dynamic normal stresses on the width of the I-beam flange b_t and the number of reinforcement bars in the tension zone of a fiber-reinforced concrete beam, taking into account the mass of the beam and without taking into account the bimodularity at $n_c = 2$.

Flange Width b_t	$n_t=2$		$n_t=4$		$n_t=6$	
	σ_{dt} , MPa	σ_{dc} , MPa	σ_{dt} , MPa	σ_{dc} , MPa	σ_{dt} , MPa	σ_{dc} , MPa
30	0,499	0,536	0,445	0,537	0,403	0,539
32	0,489	0,536	0,437	0,537	0,397	0,539
34	0,479	0,536	0,43	0,538	0,391	0,54
36	0,47	0,537	0,423	0,538	0,385	0,54
38	0,462	0,537	0,416	0,538	0,38	0,54
40	0,453	0,537	0,41	0,539	0,374	0,541
42	0,445	0,537	0,403	0,539	0,369	0,541
44	0,438	0,538	0,397	0,54	0,364	0,542
46	0,43	0,538	0,391	0,54	0,359	0,542

If the bimodularity of concrete was not taken into account (Figure 8, Table 7), the picture of the stress state changed qualitatively in comparison with the stress state when taking into account bimodularity (Figure 7, Table 6): the dynamic normal tensile stresses were less in absolute value than the dynamic normal compressive stresses.

Dependences of the dynamic normal stresses on the thickness of the flange t_f of the I-beam and the number of reinforcement rods in the tension zone of the fiber-reinforced concrete beam, taking into account the beam mass and bimodularity are presented in Figure 9 and Table 8.

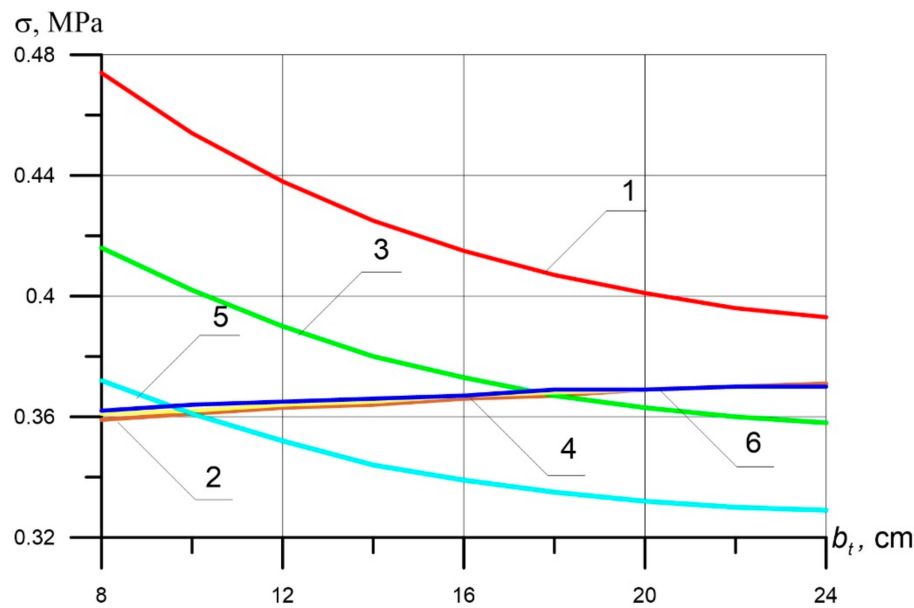


Figure 9. Dependences of the dynamic normal stresses on the thickness of the flange t_t of the I-beam and the number of reinforcement rods in the tension zone of the fiber-reinforced concrete beam, taking into account the beam mass and bimodularity at $n_c = 2$, $E_c = 2250$ MPa, $E_t = 5000$ MPa: (1) dynamic tensile stresses at $n_t = 2$; (2) dynamic compressive stress at $n_t = 2$; (3) dynamic tensile stresses at $n_t = 4$; (4) dynamic compressive stress at $n_t = 4$; (5) dynamic tensile stresses at $n_t = 6$; (6) dynamic compressive stresses at $n_t = 6$.

Table 8. Dependences of dynamic normal stresses on the thickness of the flange t_t of the I-beam and the number of reinforcement bars in the tension zone of a fiber-reinforced concrete beam, taking into account the beam mass and bimodularity at $n_c = 2$.

Flange Thickness		$n_t = 2$		$n_t = 4$		$n_t = 6$	
t_t		σ_{dtr} , MPa	σ_{dcr} , MPa	σ_{dtr} , MPa	σ_{dcr} , MPa	σ_{dtr} , MPa	σ_{dcr} , MPa
8		0.474	0.359	0.416	0.361	0.372	0.362
10		0.454	0.361	0.402	0.362	0.361	0.364
12		0.438	0.363	0.39	0.364	0.352	0.365
14		0.425	0.364	0.38	0.365	0.344	0.366
16		0.415	0.366	0.373	0.367	0.339	0.367
18		0.407	0.367	0.367	0.368	0.335	0.369
20		0.401	0.369	0.363	0.369	0.332	0.369
22		0.396	0.37	0.36	0.37	0.33	0.37
24		0.393	0.371	0.358	0.37	0.329	0.37

From the graph shown in Figure 9 and Table 8, it can be seen that with an increase in the thickness of the flange of the I-beam t_t in the stretched zone, σ_{dt} decreased, and σ_{dc} increased. A simultaneous increase in t_t by 1.5 times and in the number of reinforcement rods by 3 times decreased σ_{dt} by 45%, while σ_{dc} increased by only 3%.

Dependences of dynamic normal stresses on the thickness of the flange t_t of the I-beam and the number of reinforcement rods in the tension zone of a fiber-reinforced concrete beam, taking into account the mass of the beam and without taking into account the bimodularity, are shown in Figure 10 and Table 9.

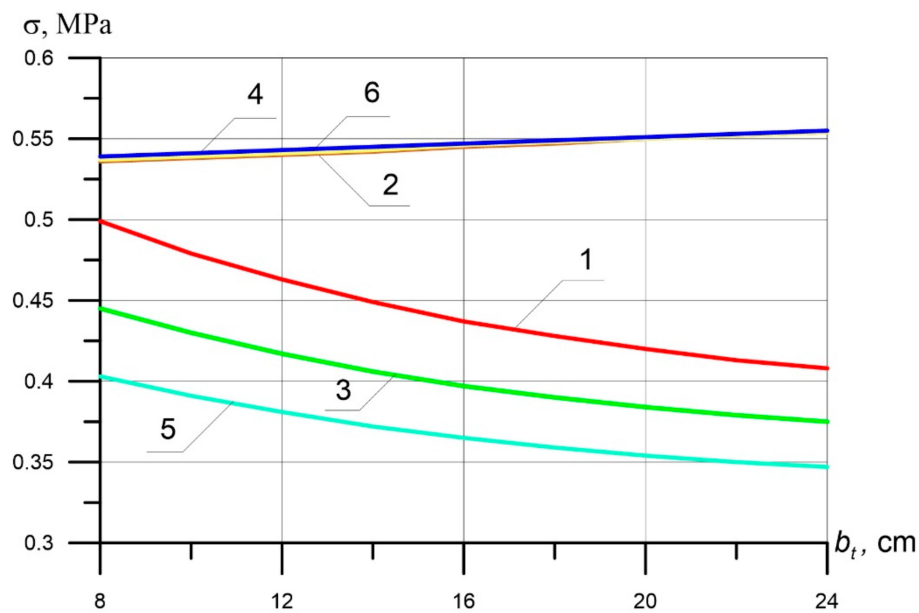


Figure 10. Dependence of the dynamic normal stresses on the thickness of the flange t_f of the I-beam and the number of reinforcement bars in the tension zone of the fiber-reinforced concrete beam, taking into account the mass of the beam and without the bimodularity at $n_c = 2$, $E_c = 5000$ MPa, $E_t = 5000$ MPa: (1) dynamic tensile stresses at $n_t = 2$; (2) dynamic compressive stress at $n_t = 2$; (3) dynamic tensile stresses at $n_t = 4$; (4) dynamic compressive stress at $n_t = 4$; (5) dynamic tensile stresses at $n_t = 6$; (6) dynamic compressive stresses at $n_t = 6$.

Table 9. Dependences of dynamic normal stresses on the thickness of the flange t_f of the I-beam and the number of reinforcement bars in the tension zone of the fiber-reinforced concrete beam, taking into account the mass of the beam and without the bimodularity at $n_c = 2$.

Flange Thickness		$n_t=2$		$n_t=4$		$n_t=6$	
t_f		σ_{dt} , MPa	σ_{dc} , MPa	σ_{dt} , MPa	σ_{dc} , MPa	σ_{dt} , MPa	σ_{dc} , MPa
8		0.499	0.536	0.445	0.537	0.403	0.539
10		0.479	0.538	0.43	0.539	0.391	0.541
12		0.463	0.54	0.417	0.541	0.381	0.543
14		0.449	0.542	0.406	0.543	0.372	0.545
16		0.437	0.545	0.397	0.546	0.365	0.547
18		0.428	0.547	0.39	0.548	0.359	0.549
20		0.42	0.55	0.384	0.55	0.354	0.551
22		0.413	0.552	0.379	0.552	0.35	0.553
24		0.408	0.554	0.375	0.554	0.347	0.555

Without taking into account bimodularity, as well as taking into account the bimodularity of the beam material, an increase in the thickness of the lower flange and an increase in the number of reinforcement led to an increase in σ_{dc} and a decrease in σ_{dt} , but $[\sigma_{dc}] > [\sigma_{dt}]$ (Figure 10, Table 9).

4. Discussion

The obtained mathematical models for calculating reinforced beams of various sections and shapes show that the bimodularity of concrete can both qualitatively and quantitatively change the stress-strain state of a structure in comparison with a homogeneous material. In our examples, a significant change in the stress state is manifested in the fact that the dynamic normal tensile stresses are lower in absolute value than the dynamic normal compressive stresses. He X.-T. et al. [3] showed, using the example of an axisymmetric plate, that the bimodular effect will significantly change the ratio of the load and the central deflection of the plate. Under the same boundary conditions, the ability to resist deformation

depends on the values of the tensile modulus of elasticity, the modulus of elasticity of the neutral layer and the modulus of elasticity in compression.

The effect of bimodularity is manifested in a change in the stress-strain state. This can be seen from the considered problems of beam bending and is typical for a complex stress state. A similar trend is discussed in the work of Shah S. et al. [38]. The authors investigated the influence of the bimodular behavior of adhesive and curing stresses on the behavior of interfacial delamination cracks in tee joints by performing sequential thermal and geometrically nonlinear finite element analysis. The authors also noted that the effect of bimodularity in comparison with the functional gradient turned out to be much more significant on the fracture behavior in the mixed mode, which indicated a slowdown in the rate of fracture propagation at the interface along certain zones.

The numerical study presented in this work shows that the stress state, taking into account the bimodularity under the action of a shock load, is qualitatively and quantitatively affected by the ratio of the elastic modulus in tension and elastic modulus in compression. For beams made of heavy concrete, for which the moduli of elasticity in tension and compression are three times higher than the corresponding moduli for lightweight concrete, the dynamic maximum stresses increase three times, which is confirmed by Hooke's law (Tables 1 and 3).

When $E_t > E_c$ in a T-section beam, regardless of the number of rods, σ_{dt} differs from σ_{dc} by only 0.7% (Tables 1 and 4). At $E_t = E_c$ $\sigma_{dc} > \sigma_{dt}$ by 57% (Table 2). In the case of $E_t < E_c$ $\sigma_{dc} > \sigma_{dt}$ by 13% (Table 3). The data presented confirm the need to take into account bimodularity when calculating the strength of beams under shock loads.

The stress state of the beam is influenced by the impact (at the same section height) and the shape of the cross-section. From the values of the maximum tensile and compressive stresses given in the tables, it can be seen that the highest stresses arise in the T-cross-section beams, the smallest in the rectangular cross-section beams, both with and without regard to the mass of the beam.

The arrangement of reinforcement bars in compression and tension zones also affects the stress state of the beam under impact. So, at $E_t > E_c$ and the same number of reinforcing bars located in the compressed and tensile zones $\sigma_{dc} < \sigma_{dt}$ by 45% for a rectangular cross-section and 15% for an I-beam cross-section (Table 1). In the absence of reinforcing bars in the compressed zone, the difference between the maximum tensile and compressive stresses increases: $\sigma_{dc} < \sigma_{dt}$ by 57% for a rectangular cross-section and by 30% for an I-section (Table 5), the value of the maximum tensile normal stress in comparison with the arrangement of reinforcing bars in both the compressed and stretched zones, the increase for a rectangular cross-section is 9% and for I-beams by 13% (Tables 1 and 5). As can be seen from the graphs shown in Figures 4 and 5, by varying the dimensions of the cross-section, it is possible to significantly reduce the values of the maximum tensile normal stresses of the cross-section that arise in the beam under the action of shock loads, taking into account the bimodularity of the material.

The method presented in the article allows, when calculating the strength and design of reinforced concrete beams under shock loads, the study of the effects of the mechanical properties of the material of the beam (bimodularity), the number of reinforcing bars and their location, the shape and size of the beam cross-section, the mass of the beam, the size and height of the drop load. The proposed methodology for the bimodularity accounting makes it possible to carry out calculations to optimize the structure from the point of view of their economic cost while meeting all the requirements for safety, strength and deformability. Solorzano G. et al. [39] used a genetic algorithm with a dominance-based competitive selection technique to solve this optimal design problem. The methodology was applied in the design of rectangular isolated reinforced concrete supports.

The dynamic problems considered in this article show that taking into account the bimodularity for beams made of heavy concrete reduces the values of the maximum normal stresses (Tables 3 and 4), in contrast to beams made of fiber-reinforced concrete (Tables 1 and 2), σ_{dt} decreases within 5%, σ_{dc} decreases within 55%, both taking into account the mass of the beam and excluding the mass of the beam. Chen et al. in [40] showed a similar effect when bimodularity not only displaced the neutral axis, which is obvious, but also changed the natural frequency of the beam vibrations.

As can be seen from Tables 2 and 4, taking into account the mass of the beam reduces the dynamic normal tensile stresses and dynamic normal compressive stresses by 300–800% for lightweight concrete, by 1029–2546% for heavy concrete without taking into account bimodularity. Considering the bimodularity (Tables 1 and 3), the mass of the beam reduces the dynamic normal tensile stresses and dynamic normal compressive stresses by 162–398% for lightweight concrete, by 347–2701% for heavy concrete. The installation of reinforcing bars in the tensile zone reduces the dynamic normal stresses, considering the bimodularity of the material for lightweight concrete, by an average of 771%. A numerical study can make it possible to determine the limits of applicability of using Equation (1), which is mainly used when calculating structural elements under the action of an impact, taking into account the bimodularity of the material of beams.

Experimental verification of the methodology for taking into account bimodularity when determining the maximum static deflection [2] included in the dynamic coefficient Formula (1), (2) showed that when taking into account bimodularity, the theoretical value of the maximum deflection differs from the experimental value by 4%, without taking into account bimodularity by 6% for steel with a difference of modules in tension and compression by 2.8%. For silumin with a difference in tensile and compressive moduli by 9.7%, the experimental deflection is less than the theoretical one, taking into account bimodularity, by 0.7%, and excluding bimodularity by 5.4%. That is, the greater the difference between the moduli of elasticity in tension and compression, the more accurate the theoretical value of deflections is given by taking into account the bimodularity of the material of the beam.

5. Conclusions

The results of the study showed that the strength of reinforced concrete beams under shock loads is affected by a wide range of both mechanical and geometric characteristics. So, if we talk about the technologically justified equality of the heights of different shapes of cross-sections with the corresponding dimensions of the thickness and width of the shelves, then the maximum tensile and compressive stresses depend on taking into account the values of the elastic moduli in tension and compression.

For lightweight concrete, in our work, fiber-reinforced concrete, for which $E_t < E_c$, the smallest tensile and compressive dynamic normal stresses arise in a beam of rectangular cross-section with and without regard to the mass of the beam (Tables 1 and 2). When designing a reinforced concrete structure, however, it is necessary to take into account the weight of the beam, since although the bearing capacity of a rectangular cross-section beam is higher than that of beams of T- and I-cross-sections, the reduced mass M is twice as large as the reduced mass of beams of I- and T-cross-sections, and this is an additional load on the columns, walls and foundations.

In beams made of heavy concrete AFB-1, $E_t > E_c$, the smallest tensile and compressive normal stresses also arise in a beam of rectangular cross-section with and without regard to the mass of the beam (Tables 3 and 4). As for lightweight concrete, the reduced mass M_B of a rectangular beam is twice as large as the reduced mass of I-beams and T-beams. If the normal tensile stresses σ_{dt} differ little in magnitude, then the normal compressive stresses σ_{dc} in a rectangular cross-section beam are 65% less than in a T-cross-section beam, and by 22% less than in an I-beam cross-section.

The stress state of the beams at the same cross-sectional height can be regulated by varying the cross-sectional dimensions in the stretched zone (Figures 4 and 5), which leads to a sharp decrease in σ_{dt} with a slight increase in σ_{dc} . The number and location of reinforcement bars also affect the stress state of beams. The arrangement of the rods only in the tensile zone has practically no effect on σ_{dc} , while σ_{dt} increases by 8% (Table 5).

The geometric dimensions of the cross-section of the beam and the number of reinforced bars significantly affect the stress state of the reinforced concrete beam. (Figure 7, Table 6, Figure 8, Table 7, Figure 9, Table 8, Figure 10, Table 9). The simultaneous increase in the width or thickness of the I-beam

flange is 1.8 times, and the number of reinforced rods in the tensioned zone leads to an increase in the normal compressive stress by 2% and a decrease in the normal tensile stress by 45%.

The proposed engineering method makes it possible to study the effect on the stress state of reinforced beams made of bimodular material under the action of shock loads, the geometric characteristics of the cross-section, the bimodularity of the material and the characteristics of reinforcement bars.

Author Contributions: Conceptualization, E.K., A.B., and G.S.; methodology, E.K., A.B., B.M., and G.S.; software, G.S., A.B. and O.P.; validation, E.K., A.B., and G.S.; formal analysis, E.K., A.B., and G.S.; investigation E.K., A.B., and G.S.; resources, B.M. and O.P.; data curation, E.K., A.B., and G.S.; writing—Original draft preparation, E.K., A.B., and G.S.; writing—Review and editing, A.B.; visualization, G.S. and A.B.; supervision, E.K., A.B.; project administration, B.M. and O.P.; funding acquisition, B.M. All authors have read and agreed to the published version of the manuscript.

Funding: This research was financially supported by the Russian Foundation for Base Research (project 18-01-00715-a).

Acknowledgments: Authors thanks to Don State Technical University, Rostov-on-Don, Russia for software and resource support.

Conflicts of Interest: The authors declare no conflict of interest.

References

1. Lyapin, A.; Beskopylny, A.; Meskhi, B. Structural Monitoring of Underground Structures in Multi-Layer Media by Dynamic Methods. *Sensors* **2020**, *20*, 5241. [\[CrossRef\]](#)
2. Beskopylny, A.; Meskhi, B.; Kadomtseva, E.; Strelnikov, G. Transverse Impact on Rectangular Metal and Reinforced Concrete Beams Taking into Account Bimodularity of the Material. *Materials* **2020**, *13*, 1579. [\[CrossRef\]](#)
3. He, X.-T.; Li, Y.-H.; Liu, G.-H.; Yang, Z.-X.; Sun, J.-Y. Nonlinear Bending of Functionally Graded Thin Plates with Different Moduli in Tension and Compression and Its General Perturbation Solution. *Appl. Sci.* **2018**, *8*, 731.
4. Cai, K.; Gaoc, Z.; Shi, J. Compliance optimization of a continuum with bimodulus material under multiple load cases. *Comput. Aided Des.* **2013**, *45*, 195–203. [\[CrossRef\]](#)
5. Goldsmith, W. *Impact: The Theory and Physical Behavior of Colliding Solids*; Arnold: London, UK, 1960; 379p. [\[CrossRef\]](#)
6. Borys, S.; Kaczmarek, W.; Laskowski, D. Selection and Optimization of the Parameters of the Robotized Packaging Process of One Type of Product. *Sensors* **2020**, *20*, 5378. [\[CrossRef\]](#)
7. Krašna, S.; Đorđević, S. Estimating the Effects of Awareness on Neck-Muscle Loading in Frontal Impacts with EMG and MC Sensors. *Sensors* **2020**, *20*, 3942. [\[CrossRef\]](#) [\[PubMed\]](#)
8. Furtado, A.; Vila-Pouca, N.; Varum, H.; Arêde, A. Study of the Seismic Response on the Infill Masonry Walls of a 15-Storey Reinforced Concrete Structure in Nepal. *Buildings* **2019**, *9*, 39. [\[CrossRef\]](#)
9. Safi, W.A.; Hibino, Y.; Kusunoki, K.; Sanada, Y.; Mukai, T. Impact of the Reinforcement Detailing on Seismic Performance of Isolated Non-structural Walls. *Buildings* **2020**, *10*, 89. [\[CrossRef\]](#)
10. Belov, N.N.; Yugov, N.T.; Kopanitsa, D.G.; Tabachenko, A.N.; Afanas'eva, S.A.; Yugov, A.A.; Arkhipov, I.N. Mathematical simulation of the behavior of materials and structural elements under multiple impact loading. *Russ. Phys. J.* **2010**, *53*, 90–97. [\[CrossRef\]](#)
11. Wu, X.; Li, W.; Zhang, Y.; Tian, W.; Su, G.; Qiu, S. Analysis of accidental loss of pool coolant due to leakage in a PWR SFP. *Ann. Nuclear Energy* **2015**, *77*, 65–73. [\[CrossRef\]](#)
12. Buzurkin, A.; Gladky, I.; Kraus, E. Determination and verification of Johnson–Cook model parameters at high-speed deformation of titanium alloys. *Aerosp. Sci. Technol.* **2015**, *45*, 121–127. [\[CrossRef\]](#)
13. Pan, K.; Yu, R.C.; Zhang, X.; Ruiz, G.; Wu, Z. Propagation Speed of Dynamic Mode-I Cracks in Self-Compacting Steel Fiber-Reinforced Concrete. *Materials* **2020**, *13*, 4053. [\[CrossRef\]](#) [\[PubMed\]](#)
14. Li, Y.; Zhai, Y.; Liang, W.; Li, Y.; Dong, Q.; Meng, F. Dynamic Mechanical Properties and Visco-Elastic Damage Constitutive Model of Freeze–Thawed Concrete. *Materials* **2020**, *13*, 4056. [\[CrossRef\]](#) [\[PubMed\]](#)
15. Yu, X.; Fu, Y.; Dong, X.; Zhou, F.; Ning, J. An Improved Lagrangian-Inverse Method for Evaluating the Dynamic Constitutive Parameters of Concrete. *Materials* **2020**, *13*, 1871. [\[CrossRef\]](#)

16. Zhai, Y.; Li, Y.; Li, Y.; Zhang, Y.; Meng, F.; Lu, M. Impact Compression Test and Numerical Simulation Analysis of Concrete after Thermal Treatment in Complex Stress State. *Materials* **2019**, *12*, 1938. [\[CrossRef\]](#)
17. Radchenko, P.; Batuev, S.; Radchenko, A.; Plevkov, V.; Kudiyakov, K. Experimental and numerical investigation of concrete structures with metal and non-metal reinforcement at impulse loadings. *J. Phys. Conf. Ser.* **2016**, *774*, 012065. [\[CrossRef\]](#)
18. Beskopylny, A.; Kadomtseva, E.; Strelnikov, G.; Shabanov, Y. Stress-strain state of a reinforced stepped bimodular column. *IOP Conf. Ser. Mater. Sci. Eng.* **2019**, *661*, 012030. [\[CrossRef\]](#)
19. Beskopylny, A.; Kadomtseva, E.; Strelnikov, G. Static analysis of a reinforced bimodulus beam on elastic foundation. *MATEC Web Conf.* **2018**, 196. [\[CrossRef\]](#)
20. Ambartsumyan, S.A. *Multimodulus Elasticity Theory*; Science: Moscow, Russia, 1982; p. 317.
21. Ambartsumyan, S.A. The basic equations and relations in the theory of elasticity of anisotropic bodies with different moduli in tension and compression. *J. Mekh. Tverd. Tela* **1969**, *3*, 51–61.
22. Ambartsumyan, S.A.; Khachatryan, A.A. Theory of weak-moment shells made from varying-modulus material. *Int. Appl. Mech.* **1969**, *5*, 447–454. [\[CrossRef\]](#)
23. Jones, R.M. Stress-strain relations for materials with different moduli in tension and compression. *AIAA J.* **1977**, *15*, 16–23. [\[CrossRef\]](#)
24. Bert, C.W. Models for fibrous composites with different properties in tension and compression. *J. Eng. Mater. Technol.* **1977**, *99*, 344–349. [\[CrossRef\]](#)
25. Zolochovsky, A.; Voyiadjis, G. Theory of creep deformation with kinematic hardening for materials with different properties in tension and compression. *Int. J. Plast.* **2005**, *21*, 435–462. [\[CrossRef\]](#)
26. Zolochovsky, A.; Galishin, A.; Sklepov, S.; Voyiadjis, G. Analysis of creep deformation and creep damage in thin-walled branched shells from materials with different behavior in tension and compression. *Int. J. Solids Struct.* **2007**, *44*, 5075–5100. [\[CrossRef\]](#)
27. Zolochovsky, A.; Martynenko, A.; Kühhorn, A. Structural benchmark creep and creep damage testing for finite element analysis with material tension–compression asymmetry and symmetry. *Comput. Struct.* **2012**, *100–101*, 27–38.
28. He, X.; Li, X.; Li, W.; Sun, J. Bending analysis of functionally graded curved beams with different properties in tension and compression. *Arch. Appl. Mech.* **2019**, *89*, 1973–1994. [\[CrossRef\]](#)
29. He, X.-T.; Wang, Y.-Z.; Shi, S.-J.; Sun, J.-Y. An electroelastic solution for functionally graded piezoelectric material beams with different moduli in tension and compression. *J. Intell. Mater. Syst. Struct.* **2017**, *29*, 1649–1669. [\[CrossRef\]](#)
30. He, X.-T.; Li, W.-M.; Sun, J.-Y.; Wang, Z.-X. An elasticity solution of functionally graded beams with different moduli in tension and compression. *Mech. Adv. Mater. Struct.* **2016**, *25*, 143–154. [\[CrossRef\]](#)
31. He, X.; Chen, Q.; Sun, J.; Zheng, Z.; Chen, S. Application of the Kirchhoff hypothesis to bending thin plates with different moduli in tension and compression. *J. Mech. Mater. Struct.* **2010**, *5*, 755–769. [\[CrossRef\]](#)
32. Li, X.; Sun, J.-Y.; Dong, J.; He, X.-T. One-Dimensional and Two-Dimensional Analytical Solutions for Functionally Graded Beams with Different Moduli in Tension and Compression. *Materials* **2018**, *11*, 830. [\[CrossRef\]](#)
33. Filin, A.P. *Applied Mechanics of a Solid Deformable Body*; Science: Moscow, Russia, 1981; Volume 3, p. 480.
34. Cox, H. On Impact on Elastic Beams. *Trans. Camb. Phil. Sol.* **1849**, *9*, 73.
35. Beskopylny, A.; Kadomtseva, E.; Strelnikov, G.; Morgun, L.; Berdnik, Y.; Morgun, V. Model of heterogeneous reinforced fiber foam concrete in bending. *IOP Conf. Ser. Mater. Sci. Eng.* **2018**, 365. [\[CrossRef\]](#)
36. Beskopylny, A.; Kadomtseva, E.E.; Strelnikov, G.P.; Berdnik, Y.A. Stress-strain state of reinforced bimodulus beam on an elastic foundation. *IOP Conf. Ser. Earth Environ. Sci.* **2017**, *90*, 12064. [\[CrossRef\]](#)
37. Beskopylny, A.; Kadomtseva, E.; Strelnikov, G. Numerical study of the stress-strain state of reinforced plate on an elastic foundation by the Bubnov-Galerkin method. *IOP Conf. Ser. Earth Environ. Sci.* **2017**, *90*, 012017. [\[CrossRef\]](#)
38. Shah, S.; Panda, S.K. Bimodularity of interface layer and curing stress coupling effects on mixed mode fracture behaviour of functionally graded tee joint. *Int. J. Adhes. Adhes.* **2017**, *75*, 74–87. [\[CrossRef\]](#)
39. Solorzano, G.; Plevris, V. Optimum Design of RC Footings with Genetic Algorithms According to ACI 318-19. *Buildings* **2020**, *10*, 110. [\[CrossRef\]](#)

40. Chen, L.Y.; Lin, P.D.; Chen, L.W. Dynamic stability of thick bimodulus beams. *Comput. Struct.* **1991**, *41*, 257–263. [[CrossRef](#)]

Publisher’s Note: MDPI stays neutral with regard to jurisdictional claims in published maps and institutional affiliations.



© 2020 by the authors. Licensee MDPI, Basel, Switzerland. This article is an open access article distributed under the terms and conditions of the Creative Commons Attribution (CC BY) license (<http://creativecommons.org/licenses/by/4.0/>).